Development of split-delay x-ray optics using Si(220) crystals at SACLA

Taito Osaka*[a], Takashi Hirano[a], Makina Yabashi[b], Yasuhisa Sano[a], Kensuke Tono[c], Yuichi Inubushi[c], Takahiro Sato[d], Kanade Ogawa[b], Satoshi Matsuyama[a], Tetsuya Ishikawa[b], Kazuto Yamauchi[a,e]
[a]Department of Precision Science and Technology, Graduate School of Engineering, Osaka University, 2-1 Yamada-oka, Suita, Osaka 565-0871, Japan; [b]RIKEN SPring-8 Center, 1-1-1 Kouto, Sayo-cho, Sayo-gun, Hyogo 679-5148, Japan; [c]Japan Synchrotron Radiation Institute (JASRI), 1-1-1 Kouto, Sayo-cho, Sayo-gun, Hyogo 679-5198, Japan; [d]Department of Chemistry, School of Science, The University of Tokyo, 7-3-1 Hongo, Bunkyo-ku, Tokyo 113-0033, Japan; [e]Research Center for Ultra-Precision Science and Technology, Graduate School of Engineering, Osaka University, 2-1 Yamada-oka, Suita, Osaka 565-0871, Japan

ABSTRACT

We proposed a split and delay optics setup with Si(220) crystals combined with Kirkpatric-Baez mirror optics for x-ray pump-x-ray probe experiments at x-ray free-electron laser facilities. A prototype of the split-delay optics and its alignment procedure were tested at BL29XUL of SPring-8. The horizontal focal profile, measured via double-beam operation, showed good spatial overlap between the split beams with an FWHM of 100 nm, near the diffraction limit at 10 keV. High throughputs of the split-delay optics of 12% (upper) and 7.4% (lower) were obtained. The throughputs can be improved to 30% and 20% by optimizing the upper and lower central energy, respectively.

Keywords: x-ray split-delay technique, x-ray pump x-ray probe, x-ray beam diagnostics, x-ray FEL,

1. INTRODUCTION

The successful operation of hard x-ray free-electron laser (XFEL) facilities such as the Linac Coherent Light Source (LCLS)[1] in the USA and SPring-8 Angstrom Compact free-electron LAser (SACLA)[2] in Japan provides novel x-ray sources with great properties of an exceptionally high intensity, nearly full transverse coherence, and femtoseconds duration. The excellent properties offer great promise for the exploration of new scientific possibilities in ultrafast science with hard x-rays. The recent development of a 50 nm focusing system[3] has generated power densities up to 10^{20} W/cm^2 that have initiated investigations of nonlinear phenomena[4, 5]. Furthermore, a two-color operation[6], which provides a pair of XFEL pulses with a time separation of up to 40 fs, enables performance of XFEL pump-XFEL probe experiments.

A split and delay optics (SDO) system installed into an XFEL facility can expand the time range up to pico or nanoseconds in which not only electric responses but also atomic configuration changes could be observed. For the soft x-ray regime, a mirror based SDO has been reported and successfully implemented[7]. A similar SDO system can be applied to hard x-ray FELs and can achieve a high throughput even for pink FELs operated by the self-amplified spontaneous emission (SASE) scheme, which have a relatively wide energy width ($\approx 10^{-3}E_0$). However, a huge system is required to obtain a large time delay because of the small critical angle in the hard x-ray regime. Furthermore, unfavorable speckles due to residual figure errors of the mirror components can be considerable. The figure error should be suppressed, even on the edge region, that is now a challenging issue. An SDO system based on Si(511)[8] or (422) crystals[9] has been reported for ultrafast x-ray photon correlation spectroscopy (XPCS)[10] experiments with hard x-rays.

*Corresponding author: osaka@up.prec.eng.osaka-u.ac.jp; phone/fax +81 6 6879 7286.

X-Ray Free-Electron Lasers: Beam Diagnostics, Beamline Instrumentation, and Applications II, edited by Stefan P. Hau-Riege, Stefan P. Moeller, Makina Yabashi, Proc. of SPIE Vol. 9210, 921009 · © 2014 SPIE · CCC code: 0277-786X/14/$18 · doi: 10.1117/12.2060238

Usage of crystal optics and Bragg diffraction leads to a large reflection angle (i.e., large time delay can be obtained with a compact system) according to Bragg's law $2d\sin\theta_B = \lambda$, where d is the lattice spacing, θ_B is the Bragg angle and λ is the wavelength. The narrow Darwin width in the energy domain of such a high-order diffraction results in high energy resolution and high longitudinal coherence. However, this also decreases the throughput. Further, in this SDO system, the Bragg angle is set near 45° and this limits the x-ray energy to 8.4 keV or 7.9 keV for the case of (511) or (422), respectively. Here we propose another SDO scheme using Si(220) crystals, which accepts a wide range of x-ray energies, 6.5–11.5 keV, and provides higher throughput. The results of the first commissioning of this prototype SDO system at BL29XUL of SPring-8 are also presented.

2. CONCEPTUAL LAYOUT & PROPERTIES

The concept of an SDO system is based on Si(220) diffraction in the Bragg geometry spectrally splitting an XFEL pulse into two replica pulses and then recombining them with a time delay. The SDO system consists of two thin crystals acting as the beam splitter (BS) and the merger (BM), two thick crystals acting as the beam reflectors (BRs) on the reflection branch (hereinafter called upper branch), and two channel-cut crystals (CCs) on the transmission branch (lower branch), as shown in Fig. 1. The time delay between the two pulses can be adjusted by linearly translating the BRs along each 2θ axis ($2\theta_1$ or $2\theta_2$). The two delay paths enable us to access a time delay of 0 that is necessary for both pump-probe experiments and photon diagnostics such as duration measurements. The time delay completely depends on the path-length difference (i.e., jitter free). The resolution is ideally expressed as $2\Delta d(1-\cos 2\theta_B)/c$, where Δd is the translation distance of the BRs and c is the speed of light. For example, a time resolution of 1 fs can be achieved with Δd of < 0.72 μm at 10 keV (θ_B = 18.8°). The replica pulses are ideally recombined coaxially into the SDO system. The co-axial geometry is suitable for not only XPCS experiments but also for combination with a focusing system based on Kirkpatric-Baez (K-B) mirror optics that has achieved the highest power density at XFEL sources owing to the high efficiency and small focal size.

Usage of Si(220) diffraction leads to a higher throughput than that of the reported SDO system using Si(422) diffraction owing to the wider Darwin width in the energy domain. Ideal throughputs for Si(111) monochromatic pulses are 30% (upper) and 20% (lower) at 10 keV with an energy separation of 0.7 eV between the upper and lower pulses, where the Si(111) and (220) Darwin widths are 1.3 eV and 0.56 eV, respectively. By setting the incident angle of each crystal component to another θ_B, 6.5–11.5 keV x-ray energy that corresponds to θ_B range of 16.3–29.8° can be achieved.

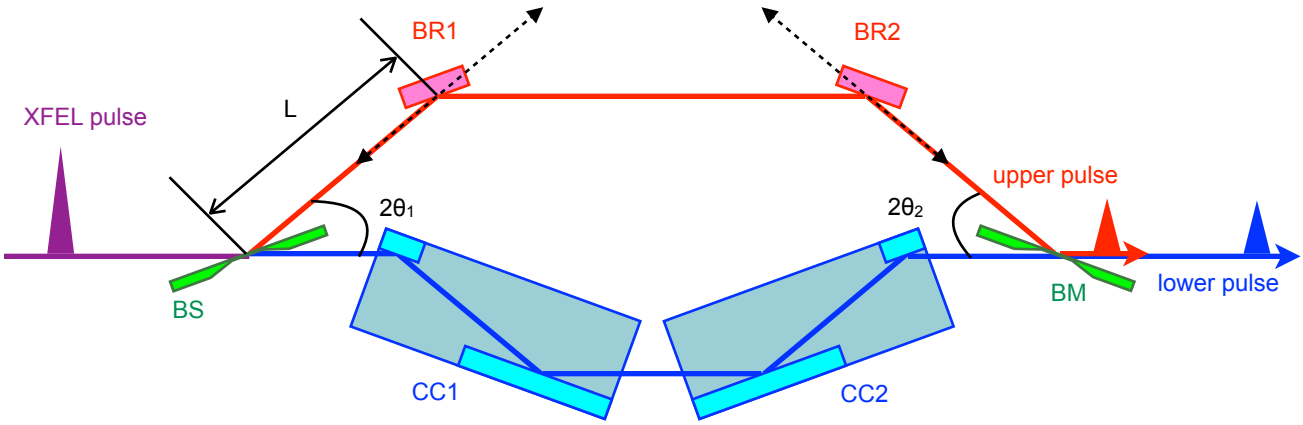

Fig. 1 Schematic of crystal layout of the split-delay optics using Si(220) crystals. BS, BRs, BM, and CCs represent the beam splitter, beam reflectors, beam merger, and channel-cut crystals, respectively. The angles between the original optical axis and the linear translation axes of the BR1 and BR2 are $2\theta_1$ and $2\theta_2$, respectively. The length between the centers of the BS and the BR1 is L.

The optical path of the lower pulse passing through each CC is perfectly parallel to the original path because the x-ray beam is reflected twice on each CC according to the parallel lattice planes. Therefore applying CCs can simplify the alignment procedure drastically.

As the BS and the BM, less than 10 μm thick, nearly perfect crystals were developed based on an etching technique using plasma at atmospheric pressure[11, 12] named plasma chemical vaporization machining (PCVM)[13]. The micro roughness of the crystals was < 0.2 nm rms. Some crystals developed by this technique have been successfully implemented at XFEL sources[14]. The inner-wall surface of the CCs were also treated by a similar PCVM technique to remove crystallographic damage on the surface such as scratches and defects that possibly induce speckles in coherent XFEL pulses. After the treatment, speckle-free four-bounced topographs were obtained over the full energy range at the 1-km-long beamline, BL29XUL[15], of SPring-8.

3. ALIGNMENT REQUIREMENTS

3.1 Tolerated spatial displacement on source plane

Operation of the SDO system at SACLA is based on combination with a K-B focusing system to investigate ultrafast phenomena induced in an extremely high density x-ray photon field. To obtain effective experimental data, the two pulses should be spatially overlapped on the focal (sample) plane under the diffraction-limited condition. A typical K-B system consists of one-dimensional horizontal and vertical elliptical mirrors. Geometrically, a spherical x-ray wave from the source point is focused at the focal point.When the x-ray wave has a source displacement of d, the focal point also shows a displacement of d/M, where M is the geometrical demagnification of the system expressed as $M = a/b$ (a is the source-mirror distance and b is the focal distance). In the future, the SDO system will be combined with the 50 nm focusing system at SACLA[3], where the diffraction-limited focal size is 55 nm (horizontal) × 30 nm (vertical) full-width

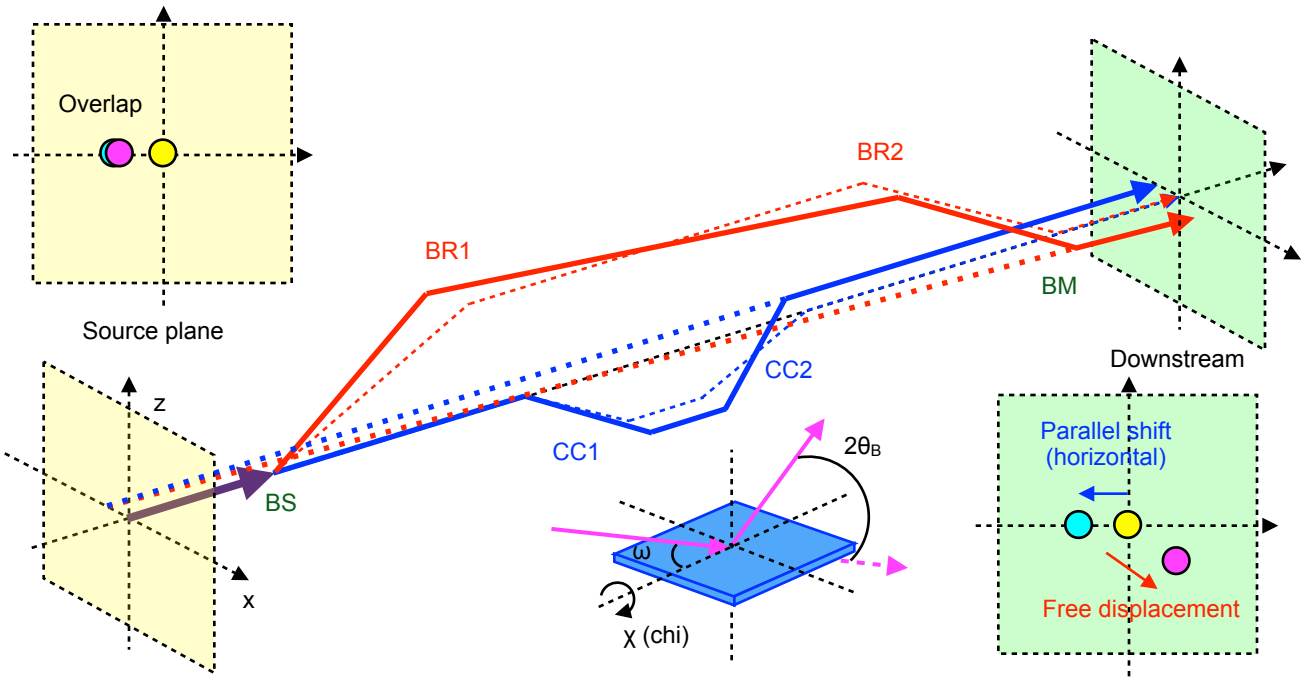

Fig. 2 Examples of beam paths passing through the split-delay optics and the relationship between the beam pointing positions on the source plane and a downstream plane. Dashed and solid lines show the ideal beam paths and practical paths, respectively. Such a path difference is caused by the miscut of crystal components and misalignment. Definitions of the rotation axes are also shown.

at half maximum (FWHM) and the geometrical demagnifications are 1324 (horizontal) and 2301 (vertical). Therefore both horizontal and vertical source displacements of 7 μm between the two pulses can be tolerated if focal displacements of 5.5 nm (horizontal) and 3.0 nm (vertical) are accepted.

3.2 Role of each crystal component

With the ideal alignment of the SDO components, both the upper and lower beams overlap on both the source and downstream planes (also on the focal plane). In practice, the two beam paths are out of the ideal paths because of the miscut of the crystal components and misalignment, as shown in Fig. 2. In this case, although beam pointing positions on a downstream plane show a displacement, the source positions overlap, which means the focal positions also overlap. This case is a solution of alignment of the SDO system combined with a K-B system. However, the two beams could possibly be out of range of the mirror acceptance. This indicates that both overlap on the source plane and parallelization of the two pulses should be accomplished. The SDO system will be placed 100 m downstream from the source at SACLA, therefore the tolerated angular error between the upper and lower pulses are estimated as 0.07 μrad.

In order to simplify such a complex system, we determined the roles of each crystal in the system. As mentioned above, the lower path is perfectly parallel to the original optical path. Note that the pointing displacement due to the miscut of the CCs occurs, as shown in Fig. 2. Geometrically, the displacement is shown only along the x (horizontal)-axis. Although the horizontal displacement can be reduced by adjusting the χ angles defined in Fig. 2, the adjustment is not necessary because an ideal alignment can be accomplished by aligning the upper-branch components (BS, BRs and BM) with reference to the lower beam. Thus, the role of the BS and the BRs is to transport the upper pulse onto the target spot on the BM where the lower pulse passes through. Parallelization of the upper beam with the lower beam is realized by adjusting only the BM. In these processes, angular errors along ω, which corresponds to the incident angle, and the χ axes present a displacement mainly along the z and x axes, respectively.

3.3 Influence of upper-branch misalignment

Here the influence of misalignment of the upper-branch components is discussed based on ray-tracing calculations in order to find a simple alignment procedure.

3.3.1 Difference between χ_{BR1} and χ_{BR2}

When all crystals satisfy the exact Bragg condition, an ideal upper-beam transportation to the target spot can be realized by adjustment of only $\chi"_{BS}$ ($\chi = \chi' + \chi"$, where χ' is the χ component of miscut and $\chi"$ is the angle of the χ-rotation stage) at an L, distance between the BS and the BR1, even with unknown χ of all crystal components. With translation of the BR1 and the BR2 along each 2θ axis (here $2\theta_1 = 2\theta_2$) that is a corresponding change in time delay, however, the upper-beam pointing spot on the BM shifts along the x axis if χ_{BR1} is not equal to χ_{BR2}. Note that the shift amount depends only on the difference between χ_{BR1} and χ_{BR2}, and responds linearly to this difference. Therefore, adjustment of either $\chi"_{BR1}$ or $\chi"_{BR2}$ is required.

3.3.2 Difference between $2\theta_1$ and $2\theta_2$

If ω and χ of all components are ideally adjusted, a displacement along the z axis on the BM is induced by the influence of an angular difference between $2\theta_1$ and $2\theta_2$. Here, even if these 2θs are not equal to the diffraction angle $2\theta_B$ without the angular difference ($2\theta_1 = 2\theta_2 \neq 2\theta_B$), the upper pulse reaches the target spot. The z coordinate on the BM responds linearly to the difference, therefore only the adjustment of either $2\theta_1$ or $2\theta_2$ is needed.

4. COMMISSIONING OF PROTOTYPICAL SPLIT-DELAY OPTICS

4.1 Experimental setup & alignment procedure

A prototype SDO system was constructed and commissioned at BL29XUL of SPring-8. The degrees of freedom of each crystal and the resolution are shown in Table 1. The range of L was 67–127 mm, corresponding to a range of time delay τ of -50 ps $< \tau <$ +48 ps at 10 keV. In this experiment, the initial setup began with L equal to 125 mm. An insufficient

Table 1 Degrees of freedom of each crystal and the resolutions with half step operation. The range of L is 67–127 mm.

Crystal	Axis	Resolution (Half step)
BS, BM	X	1.0 μm
	Z	1.0 μm
	ω	0.024 μrad
	χ	8.4 μrad
BR1, BR2	2θ	35 μrad
	L	0.25 μm
	ω	0.70 μrad
	χ	23 μrad
CC1, CC2	X	1.0 μm
	Z	1.0 μm
	ω	0.012 μrad

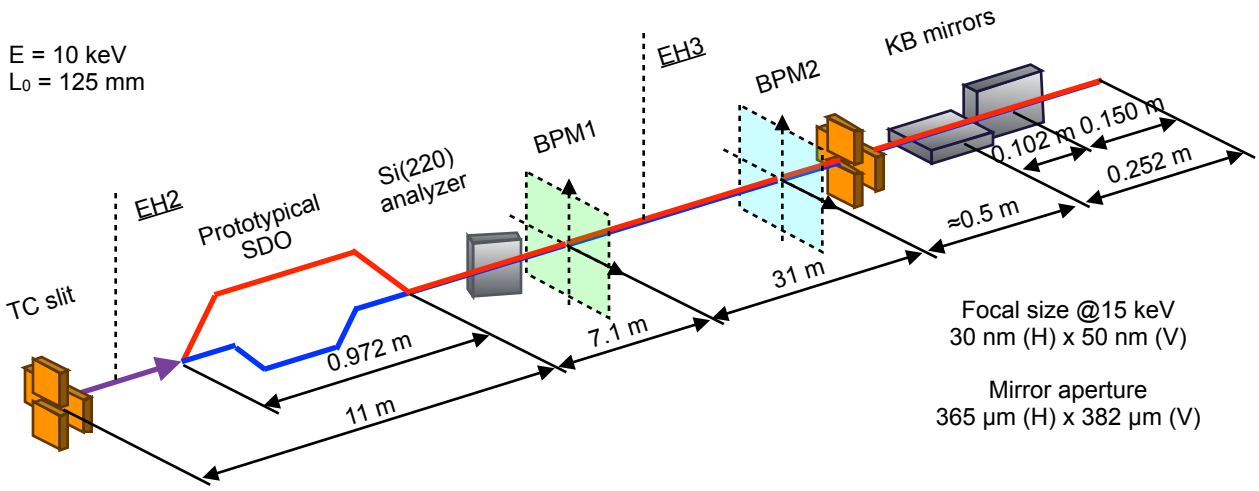

Fig. 3 Experimental setup. See text for more details.

resolution of $\chi"_{BM}$ was met by operating the rotation stage with a highly divided step motion. The experimental setup is depicted in Fig. 3. The initial test was performed with 10-keV x-rays monochromatized by a standard Si(111) double-crystal monochromator[16]. This beam line equips a K-B mirror system[17] placed 48 m downstream from a slit (TC slit) that is the virtual source and 50 m downstream from the end of the undulator. The diffraction-limited focal size is 30 nm (horizontal) × 50 nm (vertical) at 15 keV. The SDO system was placed 10 m downstream from the TC slit. In this commissioning, a Si(220) analyzer crystal in horizontal scattering geometry and two beam position monitors (BPM1: HAMAMATSU, ORCA-R2; and BPM2: BITRAN, CS-52M) were used to parallelize the upper beam. The reflection intensity from the analyzer is sensitive to the horizontal incident angle adjusted by rotating $\chi"_{BM}$. Furthermore, from the beam pointing positions of both the upper and lower beams, measured as BPM1 and BPM2 placed at two different positions, the angular error and the source displacement can be estimated.

According to the discussion in Sec. 3, a simple alignment procedure was proposed, as shown in Fig. 4. All processes were conducted online, and the analyzer and K-B mirrors were aligned with reference to the lower beam that was adjusted first. After tuning ω of the BS and BRs, adjustment of $2\theta_2$ was performed with a dummy crystal replacing the BM because the spatial acceptance of the BM is not large, especially along the z axis. Then, the upper beam was parallelized to the lower beam by means of the analyzer and two BPMs. Even when the upper beam is perfectly parallelized to the lower beam, the focal spot has a displacement and the upper beam reaches a different spot from that of the lower beam on the BM. Therefore, the pointing error is corrected by the parallel shift with rotation of $\chi"_{BS}$ and $\chi"_{BM}$ in opposite synchronization with each other (e.g., rotate $\chi"_{BS}$ +1 μrad after rotating $\chi"_{BM}$ −1 μrad). Finally, the upper-

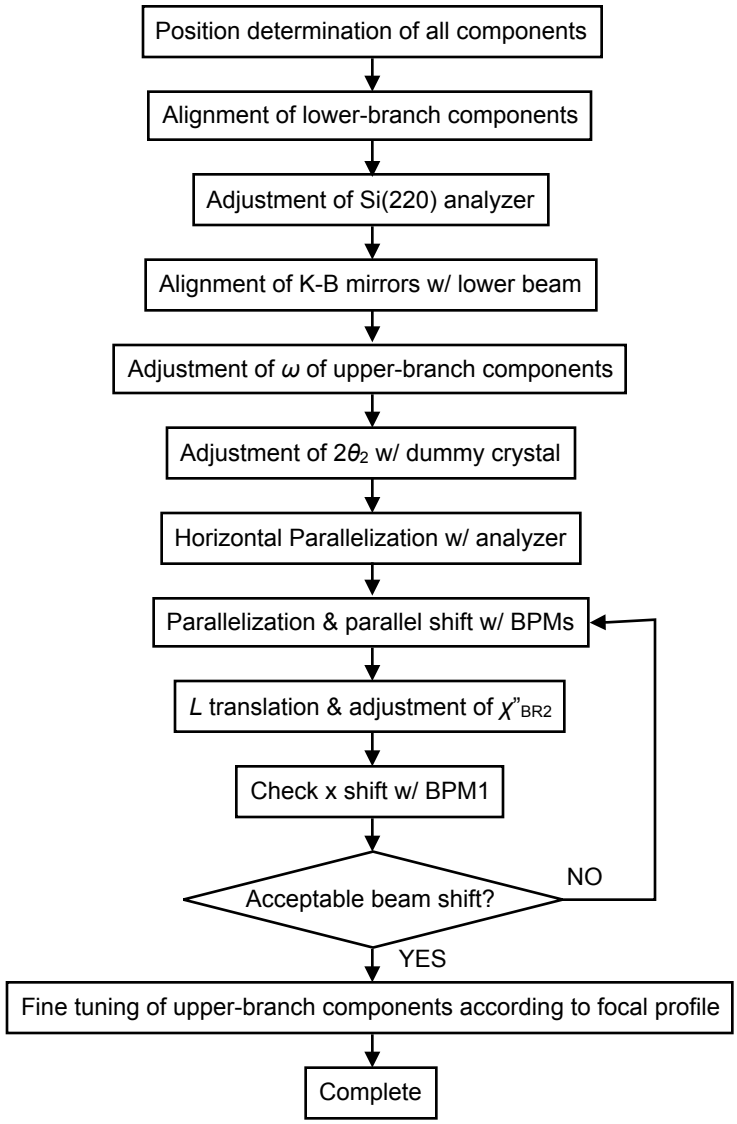

Fig. 4 Flow chart of alignment procedure.

branch components were finely tuned according to the focal profile following adjustment of χ''_{BR2}.

4.2 Results and discussions

4.2.1 Adjustment of $2\theta_2$

Figure 5 shows the results of adjustment of $2\theta_2$ with a dummy crystal, which was a thick Si(220) plate crystal. By using the dummy crystal, the upper beam could be captured on the BPM1. The upper beam before adjustment of $2\theta_2$ and the lower beam previously measured, are shown in Figs. 5(a) and 5(d). No beam distortions on either the upper or lower beams were observed. With rotation of $2\theta_2$, the upper beam moved along the z axis as expected (Figs. 5(b) and 5(c)). The z median of the upper beam was plotted in Fig. 5(e) as a function of the $2\theta_2$ rotation. The upper beam linearly shifted, where the slope was 73.12 pixel/mrad. The standard deviation of the error from the fitted line was 3.1 pixels corresponding to an ω_{BR2} error of 1.3 μrad that was due to uncertainty of the center of the rocking curve with an angular Darwin width of 19 μrad. From the slope of 224.3 μm/mrad, calculated by ray-tracing analysis, the effective pixel size of the BPM1 was estimated to be 3.07 μm, which is in good agreement with the previously measured value of 3.05 μm.

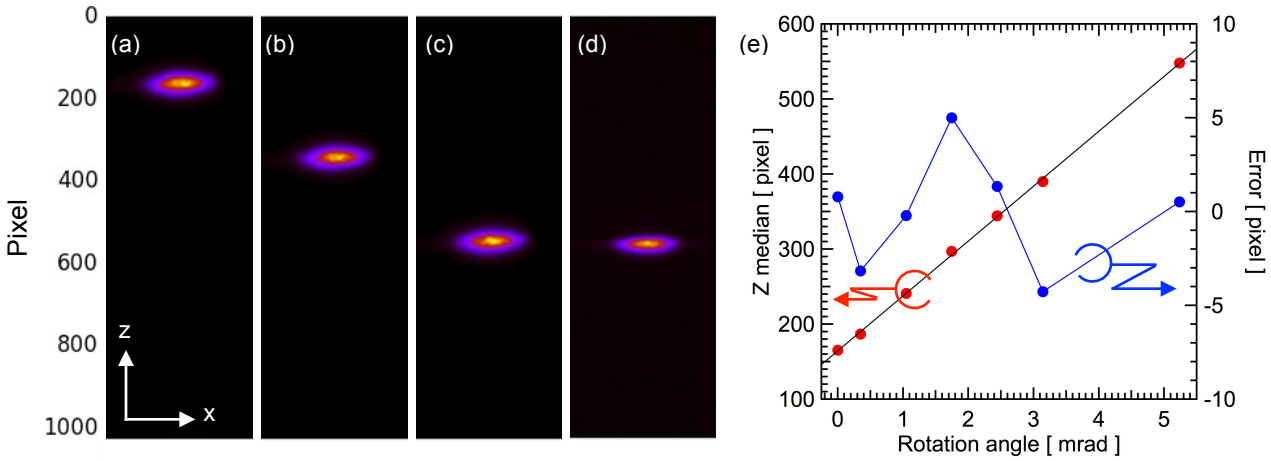

Fig. 5 (a)–(c) Upper beam profiles measured by BPM1 at a rotation of $2\theta_2$ from 0 (initial) to 2.44 and 5.24 mrad, respectively; (d) lower beam profile; (e) z medians as a function of the $2\theta_2$ rotation (red) and the errors (blue) from the linear fit (black solid line) where the slope is 73.12 pixel/mrad. The error in standard deviation is 3.1 pixel corresponding to 1.3 μrad.

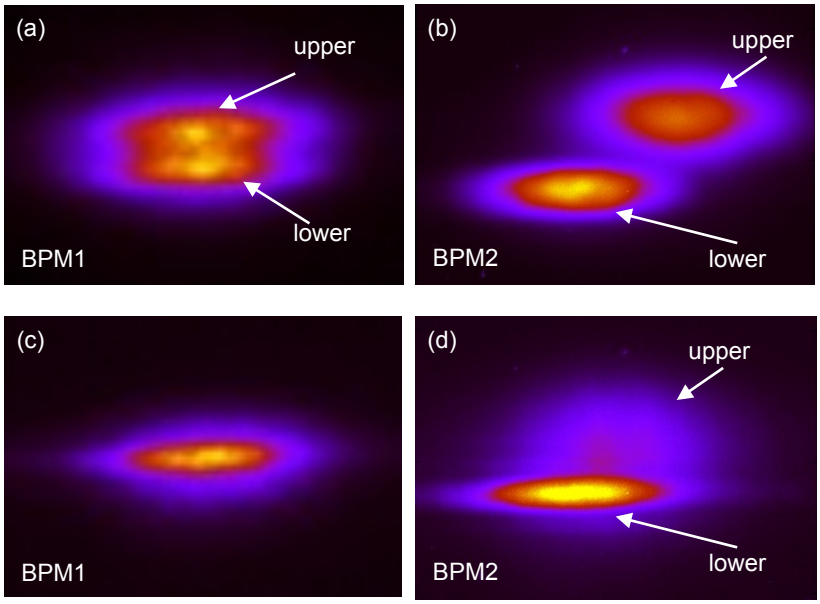

Fig. 6 Split beam profiles (a) and (b) measured after parallelization with the Si(220) analyzer on BPM1 and BPM2, respectively; (c) and (d) after parallelization and parallel shift with two BPM2. The angular errors after the two methods are +16 μrad and +3.7 μrad.

Finally, overlap of the upper beam with the lower beam along the z axis was accomplished at a sub pixel level according to the slope. These results indicate both this adjustment scheme and the ray-tracing calculation are effective for alignment of the SDO system.

4.2.2 Horizontal Parallelization and parallel shift

After adjustment of $2\theta_2$ and replacing the dummy crystal with the BM, no upper beam was captured by the BPM2 because of a large horizontal angular error. Therefore, the upper beam was parallelized with reference to the Si(220) analyzer adjusted with the lower beam. The parallelization was conducted by tuning χ"$_{BM}$ with 1/100 step operation

(0.17 μrad/pls). Owing to the adjustment, the upper and lower beams were observed on both the BPM1 and BPM2, as shown in Figs. 6(a) and 6(b). A residual horizontal angular error of +16 μrad was found to be due to angular drift of the analyzer and the energy difference between the upper and lower beams. The instability and discontinuous motion of $\chi"_{BM}$ with such a highly divided step operation was also considerable.

Next, the upper beam was parallelized according to the residual angular error estimated from the beam positions on the BPM1 and the BPM2, and then was shifted parallel. In the parallel shift, $\chi"_{BS}$ and $\chi"_{BM}$ were operated with the default step motion (half step) to stably and continuously rotate them. Beam profiles after these processes are shown in Figs. 6(c) and 6(d). A slight displacement was observed on the BPM2 although nearly full overlap was achieved on the BPM1. An angular error of +3.7 μrad remained. The cause was considered to be the instability of the χ stages. These processes were based on the center of each beam corresponding to the median. Angular errors were also estimated according to median displacements and this presumption was unobvious. Furthermore, the median calculation includes an uncertainty of a few pixels. Therefore the object parallelization is impossible by these methods even if a stable χ stage would be used.

4.2.3 Horizontal focusing

In this experiment, the upper-branch components were finely tuned according to the focal profile without adjustment of $\chi"_{BR2}$ in order to achieve spatial overlap on the focal plane. Here we focused on only the horizontal direction because

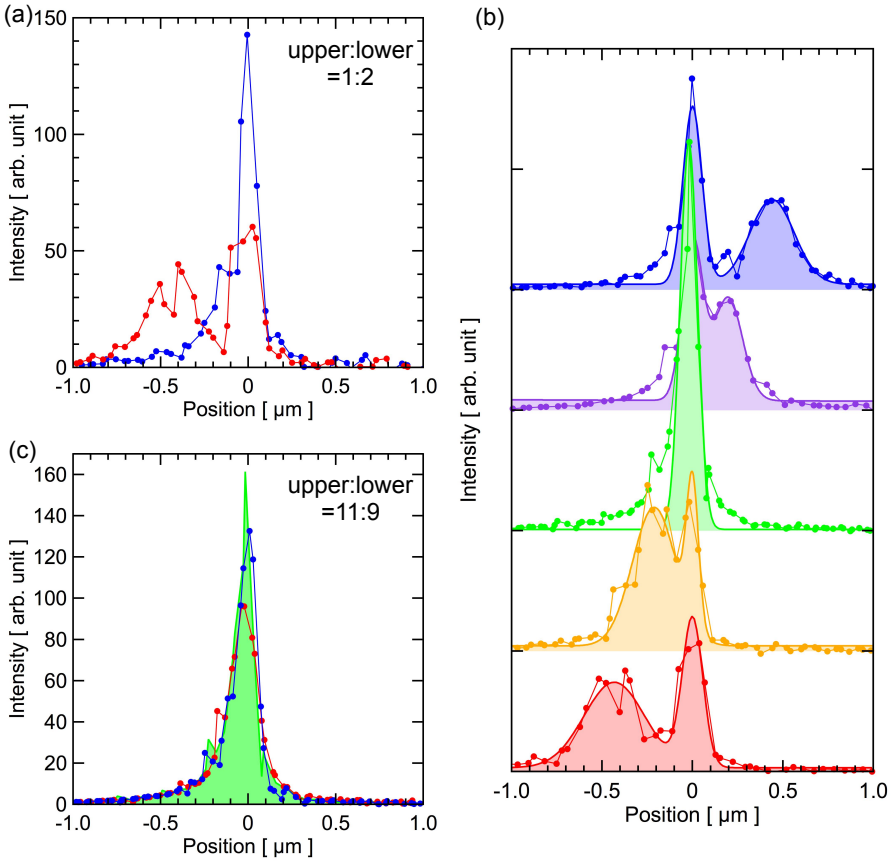

Fig. 7 Horizontal focal profiles measured with a wire scan method using a gold wire with a diameter of 1 μm. (a) Profiles measured via a two beam operation before (red) and after (blue) adjustment of $\chi"_{BM}$; (b) Two beam profiles at several upper beam shifts on the BM of –111 μm (red), –50 μm (yellow), 0 μm (green), +56 μm (purple), and +111 μm (blue); (c) Best tuned profiles measured via two beams (green filled), only upper beam (red), and only lower beam (blue). Count ratio of upper beam to lower beam measured at downstream of the K-B mirrors are 1:2 at Panel(a) and 11:9 at Panel(c).

horizontal overlap seemed to be more difficult than vertical overlap.

Initially, a horizontal focal profile with two peaks was observed (Fig. 7(a)). This result indicates that the source points of the upper and lower beams have a horizontal displacement. In the above processes, the upper beam was considered to sufficiently overlap the lower beam on the BM. Thus we attempted to overlap the upper and lower beams on the focal plane by adjusting $\chi"_{BM}$ (i.e., fine parallelization). As a result, a single peak focal profile was obtained as shown in Fig. 7(a). However, the count ratio of the upper beam to the lower beam at the downstream of the K-B mirrors was 1:2, which was lower than the output ratio of the SDO system, 5:3, that means 70% of the upper-beam flux was lost. This result indicates the source displacement was suppressed while the angular error was large, as shown in Fig. 2, and this also means that the overlap on the BM was insufficient.

Once $\chi"_{BM}$ was returned to the initial angle, the parallel shift was conducted. Figure 7(b) presents several focal profiles measured by this process. The upper-beam peak shifted linearly as a function of upper-beam translation on the BM by the parallel shift. At the best tuned position, a single peak focal profile with 100 nm FWHM, which was near the diffraction limit at 10 keV, was obtained (Fig. 7(c)). The count ratio was 11:9, a significant improvement.

4.2.4 Throughput

Throughputs without absorption by air of the upper and lower branches were 12% and 7.1%, respectively, and these values are to be compared to the ideal values that are 45% and 6.4%, respectively. The reduction of the upper-branch throughput appears to be due to dispersion by the BS because a slightly bent lattice plane of BS was observed. On the other hand, it was confirmed that the BM has a flat lattice plane. Another thin crystal with a nearly flat lattice plane has been prepared and the upper-branch throughput can be improved by replacing the BS with this crystal. Furthermore, in this experiment, the upper beam captured the central energy range of the incident beam. As mentioned in Sec. 2, optimization of central energies of the upper and lower beams can improve lower-branch throughput.

5. CONCLUSIONS & FUTURE PERSPECTIVES

We proposed an SDO system using Si(220) crystals, which can realize higher throughput than that of the reported one for the hard x-ray regime and can accept a wide range of x-ray energies, 6.5–11.5 keV. Essential crystal components, ultrathin crystals and channel-cut crystals, were developed based on the PCVM technique. A simple alignment procedure was proposed according to the results of ray-tracing calculations. Effectiveness of the procedure was confirmed by an initial test at BL29XUL of SPring-8 with a prototype SDO system. As a result of this initial test, a 100-nm-width single-peak horizontal focal profile was obtained with a slight flux loss. The throughputs of the upper and lower branches were 12% and 7.1%, respectively, which can be improved by replacing the BS with an improved crystal and by optimizing the central energies of the two beams.

In the near future, the proposed alignment procedure will be completed at SPring-8. Then, this SDO system will be used at SACLA to measure pulse duration by detecting nonlinear phenomena, such as second-harmonic generation[18] and saturable absorption[5], as a function of time delay. Furthermore, use of self-seeded FELs[19] can increase throughput of the SDO system drastically, owing to the high monochromaticity that will realize a high power density comparable with one achieved with pink FELs.

ACKNOWLEDGMENTS

The authors thank the staff of SACLA/SPring-8 for their continuous support and appreciate HXR (XPP/XCS) Dept. staff of LCLS, Dr. G. Grübel, Dr. W. Roseker, Dr. F. Lehmkuehler, and Mr. M. Walther of DESY gave us great experience of their SDO commissioning at XCS of LCLS. This study was partially supported by X-ray Free Electron Laser Priority Strategy Program from MEXT and Grant-in-Aid for JSPS Fellows from Japan Society for the Promotion of Science, 25-989.

REFERENCES

[1] Emma, P. *et al*., "First lasing and operation of an ångstrom-wavelength free-electron laser," Nature Photon. **4**, 641–647 (2010).

[2] Ishikawa, T. *et al*., "A compact X-ray free-electron laser emitting in the sub-ångström region," Nature Photon. **6**, 540–544 (2012).

[3] Mimura, H. *et al*., "Generation of 10^{20} Wcm^{-2} hard X-ray laser pulses with two-stage reflective focusing system," Nature Commun. **5**, 3539 (2014).

[4] Tamasaku, K. et al., "X-ray two-photon absorption competing against single and sequential multiphoton processes," Nature Photon. **8**, 313–316 (2014).

[5] Yoneda, H. *et al*., "Saturable Absorption of Hard X-rays in Iron," Nature Commun. to be published.

[6] Hara, T. *et al*., "Two-color hard X-ray free-electron laser with wide tunability," Nature Commun. **4**, 2919 (2014).

[7] Mitzner, R. *et al*., "Spatio-temporal coherence of free-electron laser pulses in the soft x-ray regime," Opt. Express **16**(24), 19909–19919 (2008).

[8] Roseker, W. *et al*., "Development of a hard X-ray delay line for X-ray photon correlation spectroscopy and jitter-free pump-probe experiments at X-ray free-electron laser sources," J. Synchrotron Rad. **18**, 481–491 (2011).

[9] Roseker, W. *et al*., "Hard x-ray delay line for x-ray photon correlation spectroscopy and jitter-free pump-probe experiments at LCLS," Proc. SPIE **8504**, 85040I (2012).

[10] Grübel, G. *et al*., "XPCS at the European X-ray free electron laser facility," Nucl. Instrum. Methods B **262**, 357–367 (2007).

[11] Osaka, T. *et al*., "Fabrication of ultrathin Bragg beam splitter by plasma chemical vaporization machining," Key Eng. Mater. **523–524**, 40–45 (2012).

[12] Osaka, T. *et al*., "A Bragg beam splitter for hard x-ray free-electron lasers," Opt. Express **21**, 2823–2831 (2013).

[13] Mori, Y. *et al*., "The study of fabrication of x-ray mirror by numerically controlled plasma chemical vaporization machining: development of the machine for the x-ray mirror fabrication," Rev. Sci. Instrum. **71**(12), 4620–4626 (2000).

[14] Osaka, T. *et al*., "Thin crystal development and applications for hard x-ray free-electron lasers," Proc. SPIE **8848**, 88480S (2013).

[15] Tamasaku, K. *et al*., "SPring-8 RIKEN beamline III for coherent X-ray optics," Nucl. Instrum. Methods Phys. Res. **A467–468**, 686–689 (2001).

[16] Yabashi, M. *et al*., "SPring-8 standard x-ray monochromators," Proc. SPIE **3773**, 2–13 (2003).

[17] Matsuyama, S. *et al*., "Development of scanning X-ray fluorescence microscope with spatial resolution of 30 nm using K-B mirrors optics," Rev. Sci. Instrum. **77**, 103102 (2006).

[18] Shwartz, S. *et al*., "X-Ray Second Harmonic Generation," Phys. Rev. Lett. **112**(16), 163901 (2014).

[19] Amann, J. *et al*., "Demonstration of self-seeding in a hard-x-ray free-electron laser," Nature Photon. **6**, 693–698 (2012).